Appl. Phys. B (2016) 122:140
DOI 10.1007/s00340-016-6423-y

Applied Physics B
Lasers and Optics

Spectral broadening in lithium niobate in a self-diffraction geometry using ultrashort pulses

Jayashree A. Dharmadhikari[1] · Krithika Dota[1] · Deepak Mathur[1,2] · Aditya K. Dharmadhikari[2]

Received: 4 August 2015 / Accepted: 21 April 2016 / Published online: 6 May 2016

Abstract We report on broadband light generation in the impulsive regime in an un-doped lithium niobate ($LiNbO_3$) crystal by two femtosecond laser pulses (36 fs) from a Ti-sapphire laser amplifier. We systematically investigate the role of incident intensity on spectral broadening. At relatively low incident intensity (0.7 TW cm^{-2}), spectral broadening in the transmitted beam occurs due to the combined effect of self-phase modulation and cross-phase modulation. At higher incident intensity (10.2 TW cm^{-2}), we observe generation of as many as 21 anti-Stokes orders due to coherent anti-Stokes Raman scattering in self-diffraction geometry. Moreover, we observe order-dependent spectral broadening of anti-Stokes lines that may be attributed to the competition with other nonlinear optical effects like cross-phase modulation.

1 Introduction

Generating a broad phase-locked spectrum is a prerequisite for production of ultrashort pulses. Intense, few-cycle optical pulses (of duration ~4 fs) are achieved by expanding the spectrum of a near-infrared (~800 nm) mode-locked laser externally by means of self-phase modulation (SPM) in a rare gas-filled hollow fiber [1–4]. Phase-locking different laser oscillators, as originally proposed by Hansch [5], was the earliest approach to be adopted for sub-femtosecond pulse generation. In recent years, broadband collinear Raman generation in molecular gases has been used to produce equidistant frequency sidebands that span several octaves of optical bandwidth [6–8], which are then used to synthesize optical pulses whose duration lies in the attosecond range [9]. In the near-visible spectral region, a Raman-based technique has succeeded in producing pulses as short as 1.6 fs [10]. The broadband (octave spanning) spectrum that is a consequence of such ultrashort pulses opens up possibilities of a gamut of applications in nonlinear optical microscopy and spectroscopy [11]. The mechanisms governing Raman-based pulse compression techniques are stimulated Raman scattering, coherent anti-Stokes Raman scattering (CARS) and impulsive stimulated Raman scattering (ISRS) [12–16].

In a Raman-active medium, a coherent vibrational mode may be excited by incident laser radiation, giving rise to stimulated Raman scattering (SRS). It is well known that the SRS competes and may couple with SPM [17]. The presence of both SRS and SPM may give rise to cross-phase modulation (XPM), which causes broadening of the spectrum. It is interesting to note that in the absence of any competing processes like SPM and XPM, the spectral width of SRS is generally relatively narrow due to gain narrowing [17]. Moreover, in the case of SPM, the spectral broadening involves only one incident wavelength, whereas in the case of XPM, the incident laser wavelength generates a Stokes-shifted Raman line whose width is broadened by the coupling of the incident laser radiation and the generated Raman-shifted radiation. The first experimental observation of XPM dates back to the early 1980s in an optical fiber using an intense beam of picosecond duration [18]. In later two-beam measurements, Alfano et al. [19] reported the utility of intense picosecond pulses to enhance

✉ Aditya K. Dharmadhikari
aditya@tifr.res.in

[1] Centre for Atomic and Molecular Physics, Manipal University, Manipal 576 104, India

[2] Tata Institute of Fundamental Research, 1 Homi Bhabha Road, Mumbai 400 005, India

the spectral broadening of weaker pulses co-propagating in bulk glass.

Bulk media, like glasses and crystals, exhibit advantages vis-à-vis production of extremely short pulses over gaseous targets in the simplicity of experimental setup and the possibility of generating isolated attosecond pulses due to the continuous spectrum. The disadvantage of bulk media lies in the spectrum having large angle dispersion, an inevitable consequence of the two incident beams being in a non-collinear geometry. Synthesis of high-power single-cycle pulses in the visible and ultraviolet ranges has been demonstrated using non-degenerate cascaded four-wave mixing of femtosecond pulses in fused silica [20]. Using CARS in a $KTaO_3$ crystal, broadband spectrum in the wavelength range 500–750 nm was generated and compressed to 13 fs [21]. Based on non-degenerate impulsive stimulated Raman scattering (ISRS), a broadband spectral comb was generated around the third harmonic whose spectral width was found to be more than 4000 cm^{-1} [22]. In lead tungstate ($PbWO_4$), 20 anti-Stokes and 2 Stokes orders were generated by two-color ultrashort pulses (in the transient regime) that cross at an angle of 4° [23]. More than 15 anti-Stokes and 2 Stokes orders spanning 12,000 cm^{-1}—extending from the ultraviolet to the infrared—were generated in a BBO crystal by two crossing femtosecond laser pulses [24]. There are other reports on the generation of multiple CARS in crystals by two-color femtosecond laser pulses [25, 26]. A pair of time-delayed linearly chirped pulses of sub-picosecond duration of the same color in a self-diffraction geometry succeeded in generating 40 anti-Stokes and 5 Stokes sidebands in a $PbWO_4$ crystal, with high conversion efficiency of sidebands compared to a two-color excitation scheme [27]. The advantage of using self-diffraction geometry is that it improves the temporal contrast by as much as four orders of magnitude, thereby improving the temporal quality of the pulse quite dramatically [28].

Even though generation of multiple CARS in Raman-active crystals by two-color femtosecond laser pulses has been [23–26] studied, there is only one report [29] that has demonstrated up to the 20th anti-Stokes orders in a $LiNbO_3$ crystal using two same-color pulses, with isolated pulses of 25-fs duration being obtained by angle dispersion compensation [29]. A systematic study involving the dependence of incident intensity on broadband generation is, however, still lacking. This is important, since there might be a possibility of competition with other nonlinear optical effects like SPM and XPM.

Here, we report on a systematic study carried out on broadband light generation in an un-doped $LiNbO_3$ crystal by two identical femtosecond laser pulses in a self-diffraction geometry (the ISRS regime). We investigate the role played by self- and cross-phase modulation at relatively low input intensities. At higher intensities, we report generation of 21 anti-Stokes orders in which lower orders are more broadened compared to higher orders.

2 Experimental setup

A schematic depiction of the setup used to carry out our two-beam experiments is shown in Fig. 1 (see [30] for more detailed description). The output pulses from a Ti-sapphire laser (wavelength 800 nm, 36-fs pulse duration and 1-kHz repetition rate) are split using a 50:50 beam splitter. The two beams are then steered through two pairs of mirrors, with one pair fixed on a manual translation stage (with 1 μm least count) and the other pair fixed on a motorized translation stage (with 0.1 μm least count) to generate a temporal delay.

The two beams are focused using a 1-m focal length lens (placed before the beam splitter) onto the sample. The angle between the two beams is nonzero and is varied over the range 4°–9°. A typical temporal profile of the laser pulse, measured using spectral phase interferometry for direct electric-field reconstruction (SPIDER), is also shown in Fig. 1. The SPIDER trace shows the temporal profile of the pulse as well as its phase. We adjusted the distance between the two compressor gratings so as to have a flat phase with zero value over the pulse duration. In order to maintain the flat phase, we pre-compensated for the chirp introduced by the optics (lens and beam splitter). Both the beams were ensured to be vertically polarized. The temporal delay was initially matched using second-harmonic generation [31]. Figure 1 shows two transmitted fundamental beams along with various higher-order anti-Stokes-shifted lines. The spectral measurements were taken using a fiber-coupled spectrometer (Ocean Optics USB 2000).

3 Results and discussion

We have performed two sets of experiments to observe spectral broadening in a 1-mm-thick $LiNbO_3$ sample. In the first set of measurements, we investigate the self-phase modulation (SPM)-induced broadening by increasing the incident intensity using a single beam; in the second set of experiments, we investigate the broadening in the presence of a second beam. We first discuss the results of our single-beam experiments.

We have taken measurements in which, using a single beam, we increase the incident pump intensity and monitor the spectral broadening caused by SPM. Typical results are shown in Fig. 2 along with a plot of the central wavelength as a function of incident intensity. Figure 2 also shows the corresponding spectrum. The spectral broadening due to SPM is symmetric with respect

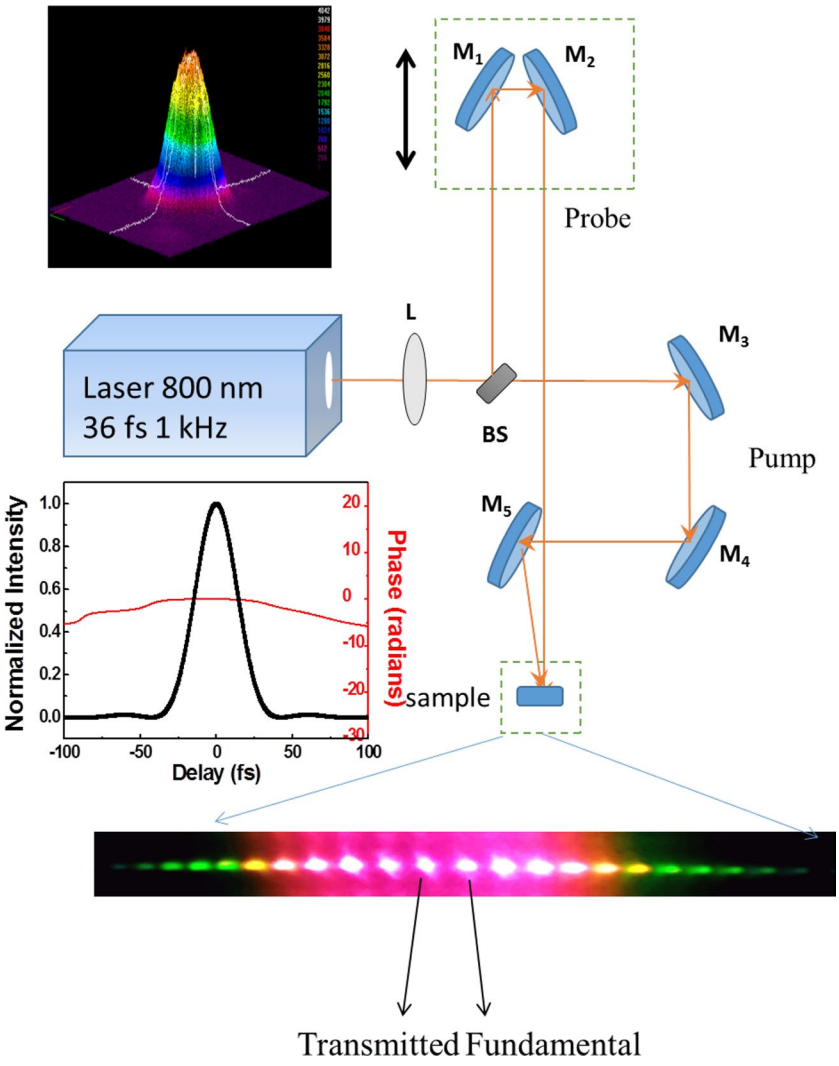

Fig. 1 Experimental setup depicting two-beam self-diffraction geometry. The laser pulses of 36 fs centered at 800 nm are obtained from a Ti-sapphire laser amplifier. Also shown are the pulse duration of the laser measured using SPIDER and the beam profile of the pulse. Image of higher-order anti-Stokes lines generated in the impulsive stimulated Raman scattering regime at zero delay position showing symmetric orders

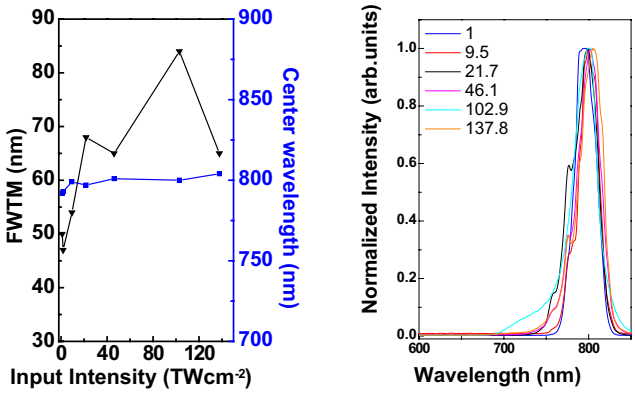

Fig. 2 *Left panel* shows the variation of spectral width (*FWTM* full width at one-tenth maximum) and center wavelength of the transmitted pump beam for different input intensities; *Right panel* shows the spectrum for corresponding intensities (in units of TW cm^{-2})

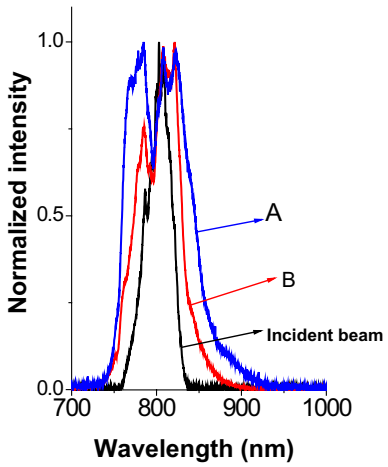

Fig. 3 Incident laser beam (*black*); spectrum A shows broadening in the first beam of 6 μJ energy (*blue*) with co-propagating second beam of 11 μJ, and spectrum B shows broadening in the second beam of 11 μJ (*red*) with co-propagating first beam of 6 μJ in $LiNbO_3$ at 4° angle between the two beams

to central wavelength of the incident beam because of the fact that time-dependent refractive index change is the same for both leading and trailing parts of the incident femtosecond pulse [17]. In Fig. 2, we do not observe any significant spectral broadening. The low spectral broadening (FWHM) due to SPM in this case may due to the fact that the bandgap of $LiNbO_3$ is less than the threshold bandgap of 4.5 eV for supercontinuum generation in bulk material [32]. Note here that the variation in FWHM is small; hence, we considered full width at one-tenth maximum (FWTM) for these measurements. It is observed that the peak wavelength does not shift even at very high intensities, up to ~138 TW cm^{-2}, whereas the spectrum itself becomes broader with increasing intensity, up to an intensity value of ~103 TW cm^{-2}. Beyond this value the spectrum narrows, because of damage caused to the sample at such high intensity values.

We now discuss results of our two-beam experiment. The two beams of same color are made incident on the sample at an angle of 4°. The interference of these two beams results in intensity modulation which, in turn, gives rise to spatial intensity variation. This changes the local refractive index, giving rise to a phase grating that diffracts the incident light beams [30]. For incident energy of 6 μJ (intensity of ~0.4 TW cm^{-2}) for the first beam and 11 μJ (intensity of ~0.7 TW cm^{-2}) for the second beam, we plot in Fig. 3 the incident laser spectrum and the transmitted spectrum of both the beams in the presence of a co-propagating beam through the $LiNbO_3$ sample. As can be seen, the incident spectrum width (FWHM) is 34 nm, but in the presence of the second beam (11 μJ), the spectral width of first beam (6 μJ) broadens quite dramatically to 86 nm (FWHM). At these energy values, only the self-diffraction orders (centered at 800 nm) are visible and there are no signatures of anti-Stoke lines in the spectrum. On the other hand, the spectral broadening of the second beam (11 μJ) in the presence of a co-propagating first beam of 6 μJ is 56 nm. When the angle between the two beams is 9°, we observe spectral broadening in the beam of 10 μJ energy with co-propagating second beam of 13 μJ energy to be 59 nm, as shown in Fig. 4. Thus, with the increase in the crossing angle, the spectral broadening is reduced due to the decrease in the overlap region of two beams. In a single-beam measurement, a spectral width of 86 nm (FWTM) is achieved at an intensity value as high as ~ 103 TW cm^{-2}, whereas addition of a second beam results in broadening of 86 nm (FWHM) at a very significantly lower intensity value (0.7 TW cm^{-2}).

In order to rationalize our observation of spectral broadening in the presence of a second beam, let us first consider the broadening mechanisms. When an intense laser pulse propagates through a transparent material,

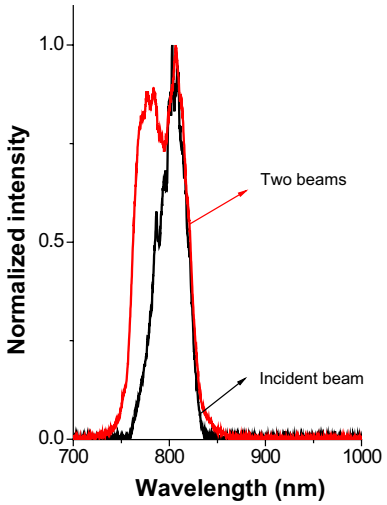

Fig. 4 Incident laser beam (*black*); spectral broadening in the beam of 10 μJ energy with co-propagating second beam of 13 μJ energy (*red*) at an angle of 9°

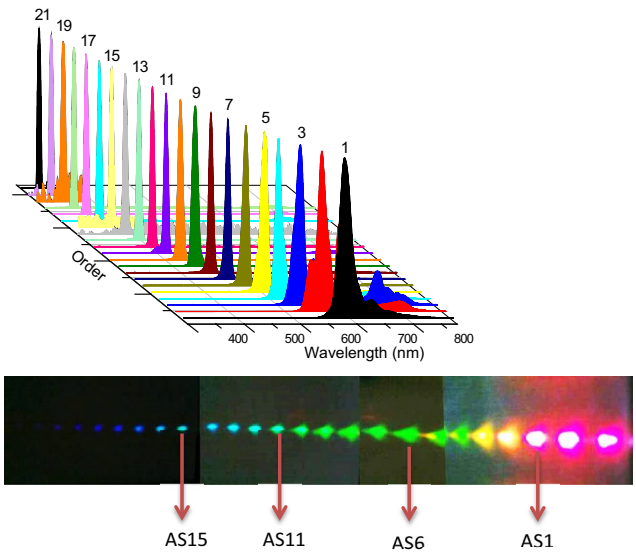

Fig. 5 Anti-Stokes orders observed in lithium niobate. Note that as many as 21 orders are generated

transient changes in the refractive index occur, resulting in changes in the phase, amplitude and frequency of the laser pulse. A time-dependent phase change causes SPM, leading to a spectral broadening [17]. When two laser pulses of different wavelengths propagate simultaneously in a medium, it results in phase modulation, amplitude modulation and spectral broadening in each pulse due to the presence of the other pulse [17]. Gersten et al. [18] have predicted that Raman spectra of ultrashort pulses would be broadened by XPM. The broadening that we observe in our measurements may be attributed to a

phenomenon similar to XPM [19]. It is interesting to note that by introduction of a second beam, the spectral width broadens by more than a factor of two compared to the incident laser spectral width.

We now discuss measurements taken at higher incident intensity in $LiNbO_3$ in the ISRS regime. In case of ferroelectric materials like lithium niobate, phonon-polariton dispersion is characterized by femtosecond time-resolved ISRS [33–36]. The experimental arrangement of ISRS in ferroelectric materials mainly consists of two ultrashort laser pulses that are temporally and spatially overlapped within the sample. This exerts a spatially periodic and temporally impulsive driving force on Raman-active modes. The frequencies of phonon-polariton modes lie within the laser pulse bandwidth (the oscillation period exceeds the laser pulse duration). In case of lithium niobate, the Raman oscillation period (300 fs) is almost ten-fold longer than the 36-fs-long incident pulse, implying that our measurements are in the ISRS regime.

On increasing the energy of the two beams to 160 μJ, we observe multicolored lines, as depicted in Fig. 5. We restricted the input energy to 160 μJ (10.2 TW cm^{-2}) in both the beams so that the peak power was kept below the critical power for self-focusing in air [37]. Figure 5 shows a spectrum of the individual 21 orders of anti-Stokes Raman lines at 4° crossing angle. When this angle is changed to 9°, we observe only 3 orders of anti-Stokes Raman lines.

It is interesting to note here that in our measurements, the peak frequency shift for the first AS1 signal is 1811 cm^{-1} which is much larger than the Raman shift (872 cm^{-1}) in the case of $LiNbO_3$. This may be because the crossing of two beams is at larger angle than required to achieve phase matching [26]. Takahashi et al. [22] have observed multiple peaks in the lower orders due to excitation of several Raman lines simultaneously by femtosecond laser pulses in their study of $YFeO_3$. The spectral profile of lower-order sidebands are, in addition, affected by the instantaneous four-wave mixing (FWM) process [22, 26]. The lower anti-Stokes orders shown in Fig. 5 have complex spectral shape that can be attributed to a FWM process superimposed on Raman sidebands. Also there is a small bending in the plane of generated beams due to the phase-matching condition [26].

We have performed calculations to lend credence to our qualitative understanding of the role of phase matching using a pair of Gaussian pulses, which are very close to those we measure in our experiments using a spectrometer. The phase-matching angle, θ, can be calculated using the following relation [38]:

$$\theta = \arccos\left[\frac{(\mathbf{k}_1+\mathbf{k}_2)^2+\mathbf{k}_3^2-\mathbf{k}_4^2}{2(\mathbf{k}_1+\mathbf{k}_2)\mathbf{k}_3}\right], \tag{1}$$

when the following phase-matching condition for $\Delta\mathbf{k}$ is satisfied:

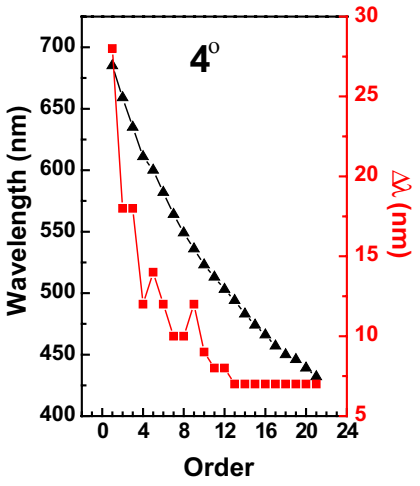

Fig. 6 Width of anti-Stokes lines for different orders (*red*). Also shown (*black*) is the plot showing the dependence of the peak wavelength on different orders

$$\Delta\mathbf{k} = \mathbf{k}_3 + \mathbf{k}_4 - \mathbf{k}_1 - \mathbf{k}_2 = 0, \tag{2}$$

where $\mathbf{k}$ is the wave vector given by

$$\mathbf{k}_i = \frac{2\pi n_i}{\lambda_i}, \tag{3}$$

where n_i is the refractive index at wavelength λ_i. The refractive index of lithium niobate, n, is calculated by using

$$n^2 - 1 = \frac{A\lambda^2}{\lambda^2 - B} + \frac{C\lambda^2}{\lambda^2 - D} + \frac{E\lambda^2}{\lambda^2 - F} \tag{4}$$

where Sellmeier coefficients $A = 2.6734$, $B = 0.01764$, $C = 1.2290$, $D = 0.05914$, $E = 12.614$ and $F = 474.6$ for $LiNbO_3$ are taken from [39]. The phase-matching angle is calculated to be 2.3° in the case of $LiNbO_3$ when the Stokes shift is 872 cm^{-1}. This angle is smaller than the angle used in our experiment, 4° and 9°. Note here that since the angle used in our experiments is greater than the phase-matching angle, the peak frequency shift observed in our experiment (1811 cm^{-1} for 4° and 2904 cm^{-1} for 9°) is greater than the Raman shift (872 cm^{-1}). In case of $LiNbO_3$, the dominant Raman line is at 872 cm^{-1}; the other Raman lines which are present are 632, 580, 432 and 250 cm^{-1}. In our measurements, we observe the presence of the 432 cm^{-1} Raman line for higher orders. Another possibility, of SPM-induced broadening of the incident pulse spectrum, contributing to the peak shift cannot be ruled out.

In Fig. 6, we plot the spectral width of the AS lines for different orders. Note here that in the initial few orders, the spectra are broadened due to competition with other nonlinear optical effects such as XPM at this high intensity used in our experiments. The side bands which are generated through the CARS process have a narrow width and

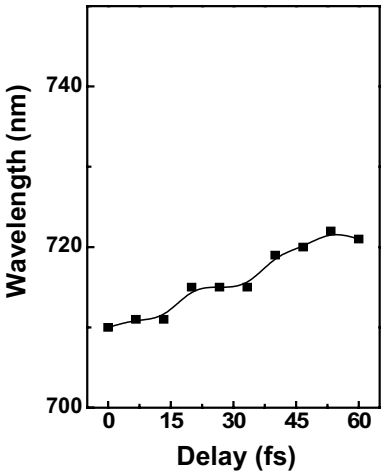

Fig. 7 Variation in the peak of the first anti-Stokes line as a function of delay

are discrete; XPM, on the other hand, gives a nearly continuous broadband spectrum. Beyond the tenth AS order, the width is reduced and thereafter remains constant. This may be because of the fact that when the pulse propagates through the crystal, it broadens, thereby reducing the intensity inside the medium.

Moreover, the pulse may also be broadened due to SPM. In Fig. 6, we also plot the peak wavelength for different anti-Stokes orders.

We have also varied the temporal delay between the two pulses of same intensity (2.5 TW cm^{-2}) so as to cause change in the modulation of the phase grating for a given crossing angle. We observe that on changing the delay by 60 fs (our incident laser pulse intensity drops to zero within 60 fs, as shown in Fig. 1), the peak wavelength of the first anti-Stokes order shifts by 10 nm (Fig. 7). This observation may be rationalized as follows [14, 40]. Through impulsive stimulated scattering, phonon-polaritons are generated by the ultrashort laser pulse. The coherent scattering (due to vibrational motion) of a second pulse occurs which is delayed relative to the first. The second pulse may, in turn, exert an impulsive force that, depending on its delay, is either in phase or out of phase with the vibrational motion induced by the first pulse. If it is in phase, the second pulse gives an additional energy to the wave and emerges redshifted. If it is out of phase, the vibrational wave loses energy to the second pulse which emerges blueshifted. Thus, the second pulse emerges out either Stokes-shifted or anti-Stokes-shifted depending on its delay. In an earlier work on amplification of anti-Stokes seed in the presence of a strong beam by XPM in fused silica [41], both positive and negative shifts of 20 nm in the peak wavelength of the anti-Stokes seed as function of delay were reported in a small window of 30 fs around zero delay [41]. The amplitude of the transient grating can also be modulated by varying the incident energy. However, we observed that variation in the incident energy does not seem to have a significant effect on the peak wavelength of the AS1 line.

The broadband spectrum that is generated in our measurement spans nearly one octave. This spectrum might be of utility after spatially overlapping all the orders and compensating the temporal chirp to obtain pulses of ~2.6-fs duration with improved temporal contrast that is intrinsic to the self-diffraction technique.

4 Summary

We have performed experiments on broadband light generation in un-doped $LiNbO_3$ when pumped by two identical femtosecond laser pulses in a self-diffraction geometry using 36-fs pulses from a Ti-sapphire laser amplifier. We observe generation of as many as 21 anti-Stokes orders in an un-doped $LiNbO_3$ sample in an impulsive SRS regime. We have systematically investigated the role of incident input intensities. At lower input energies (0.7 TW cm^{-2}), we observe broadening in the transmitted beam due to XPM; we do not observe higher-order anti-Stokes lines. At higher input intensities (10.2 TW cm^{-2}), we observed higher-order anti-Stokes lines that are broadened, with the broadening being dependent on order (up to 10th order), due to other competing nonlinear optical effects such as XPM.

Acknowledgments We thank the Department of Science and Technology for support to JAD under the Women Scientists Scheme and to DM for the J. C. Bose National Fellowship.

References

1. R.L. Fork, C.H. Brito-Cruz, P.C. Becker, C.V. Shank, Opt. Lett. **12**, 483 (1987)
2. A. Baltuska, Z. Wei, S. Pshenichnikov, D.A. Wiersman, Opt. Lett. **22**, 102 (1997)
3. M. Nisoli, S. DeSilvestri, O. Svelto, R. Szipocs, K. Ferencz, Ch. Spielmann, S. Sartania, F. Krausz, Opt. Lett. **22**, 522 (1997)
4. G. Steinmeyer, D.H. Sutter, L. Gallmann, N. Matuschek, U. Keller, Science **286**, 1507 (1999)
5. T.W. Hansch, Opt. Commun. **80**, 71 (1990)
6. S. Yoshikawa, T. Imasaka, Opt. Commun. **96**, 94 (1993)
7. H. Kawano, Y. Hirakawa, T. Imasaka, IEEE J. Quantum Electron. **34**, 260 (1998)
8. A.V. Sokolov, S.E. Harris, J. Opt. B **5**, R1 (2003)
9. A.V. Sokolov, M.Y. Shverdin, D.R. Walker, D.D. Yavuz, A.M. Burzo, G.Y. Yin, S.E. Harris, J. Mod. Opt. **52**, 285 (2005)
10. M.Y. Shverdin, D.R. Walker, D.D. Yavuz, G.Y. Yin, S.E. Harris, Phys. Rev. Lett. **94**, 033904 (2005)
11. K. Isobe, A. Suda, M. Tanaka, H. Hashimoto, F. Kannari, H. Kawano, H. Mizuno, A. Miyawaki, K. Midorikawa, IEEE J. Sel. Top. Quant. Electron. **16**, 767 (2010)

12. E.J. Woodbury, W.K. Ng, Proc. IRE **50**, 2347 (1962)
13. P.D. Maker, R.W. Terhune, Phys. Rev. **137A**, 801 (1965)
14. Y. Yan, E.B. Gamble Jr, K.A. Nelson, J. Chem. Phys. **83**, 5391 (1985)
15. A.M. Weiner, D.E. Leaird, G.P. Wiederrecht, K.A. Nelson, J. Opt. Soc. Am. B **8**, 1264 (1991)
16. A.M. Weiner, D.E. Leaird, G.P. Wiederrecht, K.A. Nelson, Science **247**, 1317 (1990)
17. R.R. Alfano, P.P. Ho, IEEE J. Quantum Electron. **24**, 351 (1988)
18. J. Gersten, R. Alfano, M. Belic, Phys. Rev. A **21**, 1222 (1980)
19. R. Alfano, Q. Wang, T. Jimbo, P. Ho, Phys. Rev. A **35**, 459 (1987)
20. R. Weigand, J.T. Mendonca, H.M. Crespo, Phys. Rev. A **79**, 063838 (2009)
21. E. Matsubara, Y. Kawamoto, T. Sekikawa, M. Yamashita, Opt. Lett. **34**, 1837 (2009)
22. J. Takahashia, Y. Kawabea, E. Hanamura, Opt. Express **12**, 1185 (2004)
23. M. Zhi, A.V. Sokolov, Opt. Lett. **32**, 2251 (2007)
24. J. Liu, J. Zhang, T. Kobayashi, Opt. Lett. **33**, 1494 (2008)
25. H. Matsuki, K. Inoue, E. Hanamura, Phys. Rev. B **75**, 024102 (2007)
26. M. Zhi, X. Wang, A.V. Sokolov, Opt. Express **16**, 12139 (2008)
27. M. Zhi, A.V. Sokolov, New J. Phys. **10**, 025032 (2008)
28. J. Liu, K. Okamura, Y. Kida, T. Kobayashi, Opt. Express **18**, 22245 (2010)
29. E. Matsubara, T. Sekikawa, M. Yamashita, Appl. Phys. Lett. **92**, 071104 (2008)
30. K. Dota, J.A. Dharmadhikari, D. Mathur, A.K. Dharmadhikari, App. Phys. B **107**, 703 (2012)
31. A.K. Bhowmik, S. Tan, A.C. Ahyi, J.A. Dharmadhikari, A.K. Dharmadhikari, D. Mathur, Opt. Commun. **280**, 472 (2007)
32. A. Brodeur, S.L. Chin, J. Opt. Soc. Am. B **16**, 637 (1999)
33. Timothy F. Crimmins, Nikolay S. Stoyanov, K.A. Nelson, J. Chem. Phys. **117**, 2882 (2002)
34. D.H. Auston, M.C. Nuss, IEEE J. Quantum Electron. **24**, 184 (1988)
35. P.C.M. Planken, L.D. Noordam, J.T.M. Kennis et al., Phys. Rev. B **45**, 7106 (1992)
36. T.P. Dougherty, G.P. Wiederrecht, K.A. Nelson, J. Opt. Soc. Am. B **9**, 2179 (1992)
37. P. Polynkin, M. Kolesik, Phys. Rev. A **87**, 053829 (2013)
38. A. Penzkofer, H.J. Lehmeier, Opt. Quantum Electron. **25**, 815 (1993)
39. D.E. Zelmon, D.L. Small, D. Jundt, J. Opt. Soc. Am. B **14**, 3319 (1997)
40. J.P. Heritage, Appl. Phys. Lett. **34**, 470 (1979)
41. J. Liu, T. Kobayashi, Sensors **10**, 4296 (2010)